J. Phys. B: At. Mol. Opt. Phys. **31** (1998) 4387–4399. Printed in the UK PII: S0953-4075(98)92879-6

State-selective electron capture in the interactions of partially stripped ions of beryllium and boron with atomic hydrogen in the ground state

M Das†, M Purkait and C R Mandal

Department of Physics, Jadavpur University, Calcutta 700 032, India

Received 31 March 1998, in final form 26 June 1998

Abstract. The Coulomb–Born approximation has been employed to study charge transfer cross sections in the case of collisions of Be^{q+} ($q = 1$–3) and B^{q+} ($q = 1$–4) with atomic hydrogen in its ground state, respectively, within the energy range of 25–200 keV amu^{-1}. The interaction of the active electron with the incoming projectile ion has been approximated by a model potential. Cross sections for capture into different sub-shells have been given in tabular form. Computed total capture cross sections compare favourably with existing available results.

1. Introduction

During the last two decades, a great deal of theoretical and experimental investigation [1–8] has been performed on charge transfer processes involving multicharged ions and atoms due to their interdisciplinary applications, namely in atmospheric physics, astrophysics, fusion research, etc. Recently, high-Z atoms such as Ni, Fe and Mo have been chosen to be the surface material for tokamak devices. As a result, impurity ions of different degree of such atoms penetrate into the plasma by sputtering. As the electron capture cross sections of such ions are high, due to high values of charge, problems gradually arise regarding stability, fuelling, etc of the inside plasma. Very recently beryllium and boron have been identified as plasma facing materials, replacing older ones in next-step fusion reactors such as ITER. For this reason a very accurate atomic database of charge transfer cross sections, involving different degree ions of beryllium and boron with atomic hydrogen, is required over the entire range of the energy region. Accurate charge transfer cross sections for collisions of fully stripped ions of Be, B, C, N, etc with atomic hydrogen are available in the literature [9–12]. In contrast, very few data [13–16] are available for the charge transfer cross sections involving such partially stripped ions with atomic hydrogen.

Olson and Salop [13] have employed the classical trajectory Monte Carlo (CTMC) method to study charge transfer cross sections in collisions of B^{q+}, C^{q+}, N^{q+} and O^{q+} ($q \geqslant 3$) with atomic hydrogen. However, charge transfer cross sections into different sub-shells for each ion are not available from their calculations. Eichler *et al* [14] has calculated charge transfer cross sections in collisions of different degree ions of Li, C, N and O with atomic hydrogen within the Oppenheimer–Brinkman–Kramers (OBK) approximation. Multiplying the OBK cross sections by a reduction factor obtained from the eikonal approximation [17] yielded final results in close agreement with experimental

† Present address: Department of Physics, Panskura Banamali College, Panskura, Midnapur, West Bengal, India.

0953-4075/98/194387+13$19.50

observations [6]. Hansen and Dubois [15] have confined their calculations to closed-shell or sub-shell ions of boron (only as a projectile). They have formulated the problem of $B^{q+}+H$ and He ($q = 1, 3, 5$) interactions respectively into the framework of the two-centre atomic state expansion method for the energy range of 0.1–100 keV amu^{-1}. State-selective electron capture cross sections are available from their investigations. Schultz *et al* [16] have calculated all the inelastic cross sections in collisions of Be^{q+} ($q = 2$–4) with atomic and molecular hydrogen in the impact energy range of 1 keV amu^{-1} to 1 MeV amu^{-1} using the CTMC method. However, charge transfer cross sections into each individual subshell are given in tabular form.

Under the prevailing circumstances, we are motivated to study charge transfer cross sections in collisions of Be^{q+} ($q = 1$–3) and B^{q+} ($q = 1$–4) with ground state atomic hydrogen within the energy range of 25–200 keV amu^{-1}. In this specified energy range, different perturbative methods are generally employed to study charge transfer reactions. The strength and weakness of such perturbative methods applied in studies of energetic ion–atom collisions have been well described by Dewangan and Eichler [18] in their review article. We have formulated our problem within the framework of the Coulomb–Born (CB) approximation. The essence of the approximation has been well understood after the formulation of the boundary-corrected first Born (B1B) [19] approximation. Applications [20–23] of the CB approximation in both three- and four-body processes have received considerable success in depicting experimental observations.

The organization of the paper is as follows. The theoretical formulation is described in section 2. Results and discussions are the contents of section 3. Finally, the paper ends with concluding remarks in section 4. Atomic units are used unless otherwise stated.

2. Theoretical formulation

The coordinate system for the charge transfer reaction

$$X^{q+} + H(1s) \rightarrow X^{(q-1)+}(nl) + H^{+}$$

is shown in figure 1, where X^{q+} represents Be^{q+} ($q = 1$–3) and B^{q+} ($q = 1$–4) ions, respectively. The total Hamiltonian of the whole system may be written as

$$H = H_0 + V_{Te}(\boldsymbol{r}_T) + V_{Pe}(\boldsymbol{r}_P) + V_{TP}(\boldsymbol{R}) \tag{1}$$

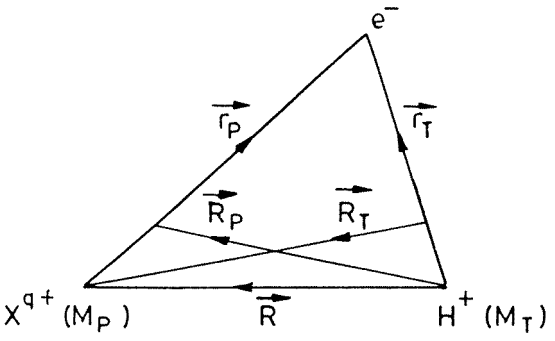

Figure 1. Coordinate representation for the reaction $X^{q+}\left(Be^{(1-4)+}/B^{(1-5)+}\right) + H(1s) \rightarrow X^{(q-1)+}(nl) + H^{+}$.

where

$$H_0 = -\frac{1}{2\mu_i}\nabla^2_{R_T} - \frac{1}{2a}\nabla^2_{r_T} \qquad \text{(entrance channel)} \tag{2a}$$

$$= -\frac{1}{2\mu_f}\nabla^2_{R_P} - \frac{1}{2b}\nabla^2_{r_P} \qquad \text{(exit channel)}. \tag{2b}$$

a, b, μ_i and μ_f are the reduced masses associated with relative coordinates $\boldsymbol{r}_T, \boldsymbol{r}_P, \boldsymbol{R}_T$ and $\boldsymbol{R}_P$, respectively. V represents the pair interaction labelled by subscripts in a charge transfer reaction where e, T and P represent the active electron, target ion and projectile ion, respectively.

Constructions of these two-body potentials and final bound state wavefunctions are constructed as follows. $V_{Te}(\boldsymbol{r}_T)$ is determined uniquely by Coulomb interaction, i.e. $V_{Te}(\boldsymbol{r}_T) = -1/r_T$. The interaction of the active electron with the projectile ion of charge 'q' has been described in three different ways: (i) the projectile ion has been treated as a rigid core ion of charge Z_P, which is determined by binding energy screening (BES) [24, 25], i.e. $Z_P = \left(-2n_f^2\varepsilon_f\right)^{1/2}$, where ε_f is the binding energy of the electron in the final state represented by principal quantum number n_f. The corresponding final state is hydrogenic with effective charge Z_P. (ii) With the same assumption, Z_P is determined by Slater screening (SS) [24, 25], i.e. $Z_P = Z - \sigma$, where Z is the nuclear charge of the projectile and σ [26] is the total screening by passive electrons. (iii) In other cases, the interaction of the active electron with the projectile ion has been approximated by a model potential as

$$V_{Pe}(\boldsymbol{r}_P) = -\frac{q}{r_P} - \frac{e^{-\lambda r_P}}{r_P}\{(Z-q) + br_P\} \tag{3}$$

where Z and q are, respectively, the nuclear and asymptotic charge of the projectile ion. b and λ are two arbitrary parameters chosen variationally in such a way that the model Hamiltonian of the active electron reproduces correct binding in the final state with respect to a Slater basis set. These binding energies have been taken from the tables of Clementi and Roetti [27] and the works of Clark and Abdallah [28]. Potential parameters for different ions are given in table 1. It may be mentioned that for the closed-shell/sub-shell structure of the projectile ion, a set of model potential parameters for a particular projectile ion reproduces excited energies with better accuracy in comparison to the case of the open-shell structure of the projectile ion. However, the accuracies of the final state wavefunctions have been tested by the virial theorem and have been found to be accurate to within 0.01%. The interaction of the projectile ion with the target nucleus has been treated as Coulombic. This is well justified as even if some short-range interaction exists charge transfer cross sections will not be affected.

Table 1. Model potential parameters λ and b in equation (3) are given for different ions.

Ion	λ	b
Be^+	2.3292	3.8616
Be^{2+}	4.3792	3.4616
Be^{3+}	6.5792	2.3446
B^+	2.1435	4.4119
B^{2+}	3.4012	5.8235
B^{3+}	6.2512	5.8616
B^{4+}	7.0512	8.2616

With all these interactions under consideration, channel Hamiltonians and interactions may be written as

entrance channel:

$$H_i = -\frac{1}{2\mu_i}\nabla^2_{R_\mathrm{T}} - \frac{1}{2a}\nabla^2_{r_\mathrm{T}} - \frac{1}{r_\mathrm{T}} \tag{4a}$$

$$V_i = \frac{q}{R} - \frac{q}{r_\mathrm{P}} - \frac{\mathrm{e}^{-\lambda r_\mathrm{P}}}{r_\mathrm{P}}\{(Z-q) + br_\mathrm{P}\} \tag{4b}$$

exit channel:

$$H_f = -\frac{1}{2\mu_f}\nabla^2_{R_\mathrm{P}} - \frac{1}{2b}\nabla^2_{r_\mathrm{P}} + \frac{(q-1)}{R} - \frac{q}{r_\mathrm{P}} - \frac{\mathrm{e}^{-\lambda r_\mathrm{P}}}{r_\mathrm{P}}\{(Z-q) + br_\mathrm{P}\} \tag{4c}$$

$$V_f = \frac{1}{R} - \frac{1}{r_\mathrm{T}}. \tag{4d}$$

The corresponding transition matrix element may be written as

$$T_{if} = \langle \chi_f^- | V | \Psi_i \rangle \tag{5}$$

where

$$V = V_i \text{ (prior) or } V_f \text{ (post)}, \tag{6}$$

Ψ_i and χ_f^- are defined by

$$(E - H_i)\Psi_i = 0 \tag{7a}$$

$$(E - H_f)\chi_f^- = 0. \tag{7b}$$

The solution for Ψ_i and χ_f^- may be written as

$$\Psi_i = \mathrm{e}^{\mathrm{i}\boldsymbol{k}_i\cdot\boldsymbol{R}_\mathrm{T}}\Phi_i(\boldsymbol{r}_\mathrm{T}) \tag{8a}$$

$$\chi_f^- = \mathrm{e}^{-\pi\alpha/2}\Gamma(1-\mathrm{i}\alpha)\mathrm{e}^{\mathrm{i}\boldsymbol{k}_f\cdot\boldsymbol{R}_\mathrm{P}}\,{}_1F_1(\mathrm{i}\alpha; 1; -\mathrm{i}(k_f R_\mathrm{P} + \boldsymbol{k}_f\cdot\boldsymbol{R}_\mathrm{P}))\Phi_f(\boldsymbol{r}_\mathrm{P}) \tag{8b}$$

where $\phi_i(\boldsymbol{r}_\mathrm{T})$ ($\phi_f(\boldsymbol{r}_\mathrm{P})$) is the initial (final) bound state wavefunction.

Using the integral representation of a confluent hypergeometric function and choosing either form of interaction potential, the transition matrix (T_{if}) may be written in a general form as

$$T_{if} = C\mathrm{e}^{-\pi\alpha/2}\Gamma(1+\mathrm{i}\alpha)\lim_{\varepsilon_1\to 0} D(\varepsilon_1, \beta, \lambda)\frac{1}{2\pi\mathrm{i}}\oint \mathrm{d}t\, t^{-\mathrm{i}\alpha-1}(t-1)^{\mathrm{i}\alpha} J \tag{9}$$

where C is some constant originating from the initial and final bound state wavefunctions, $D(\varepsilon_1, \beta, \lambda)$ is an approximate parametric differential operator,

$$J = \int \mathrm{d}\boldsymbol{r}_\mathrm{P}\cdot\mathrm{d}\boldsymbol{R}_\mathrm{P}\,\mathrm{e}^{-\mathrm{i}\boldsymbol{k}_f\cdot\boldsymbol{R}_\mathrm{P}}\frac{\mathrm{e}^{-\lambda r_\mathrm{P}}}{r_\mathrm{P}}\frac{\mathrm{e}^{-\varepsilon R_\mathrm{P}}}{R_\mathrm{P}}\mathrm{e}^{\mathrm{i}\boldsymbol{k}_f\cdot\boldsymbol{R}_\mathrm{P}t}\mathrm{e}^{\mathrm{i}\boldsymbol{k}_i\cdot\boldsymbol{R}_\mathrm{T}}\frac{\mathrm{e}^{-\beta r_\mathrm{T}}}{r_\mathrm{T}} \tag{10}$$

and $\varepsilon = \varepsilon_1 - \mathrm{i}k_f t$.

Taking a Fourier transform of terms involving r_T, r_P and R_P, and using the properties of delta-function, J may be reduced as

$$J = \frac{8}{b^2}\int \frac{\mathrm{d}\boldsymbol{Q}}{\{|\boldsymbol{Q}-\boldsymbol{q}_1|^2 + \mu_1^2\}\{|\boldsymbol{Q}-\boldsymbol{q}_2|^2 + \mu_2^2\}(Q^2+\beta^2)} \tag{11}$$

where

$$\boldsymbol{q}_1 = \left(\frac{1}{b} - a\right)\boldsymbol{k}_i \tag{12a}$$

$$\boldsymbol{q}_2 = (1-t)\boldsymbol{k}_f - a\boldsymbol{k}_i \tag{12b}$$

$$\mu_1 = \frac{\lambda}{b} \qquad \mu_2 = \varepsilon_1 - \mathrm{i}k_f t_3. \tag{12c}$$

Using the integral representation of a general three denominator integral of Lewis [29], J may be reduced in a form as

$$J = \frac{16\pi^2}{b^2}\int_0^\infty \frac{\mathrm{d}x}{A+Bt}. \tag{13}$$

So the transition amplitude may be written as

$$T_{if} = C\mathrm{e}^{-\pi\alpha/2}\Gamma(1+\mathrm{i}\alpha)\lim_{\varepsilon_1\to 0} D(\varepsilon_1,\beta,\lambda)\frac{16\pi^2}{b^2}\int_0^\infty \mathrm{d}x\frac{1}{2\pi\mathrm{i}}\oint \mathrm{d}t\, t^{-\mathrm{i}\alpha-1}(t-1)^{\mathrm{i}\alpha}\frac{1}{A+Bt}. \tag{14}$$

Now the complex integration may be evaluated by applying Cauchy's residue theorem to obtain the final form of transition matrix element (T_{if}) as

$$T_{if} = C\mathrm{e}^{-\pi\alpha/2}\Gamma(1+\mathrm{i}\alpha)\frac{16\pi^2}{b^2}\lim_{\varepsilon_1\to 0} D(\varepsilon_1,\beta,\lambda)\int_0^\infty \mathrm{d}x\, A^{-\mathrm{i}\alpha-1}(A+B)^{\mathrm{i}\alpha}. \tag{15}$$

This one-dimensional integration over transition amplitude and integration over scattering angles is performed numerically using the 48- and 24-point Gauss Legendre quadrature method, respectively, with an accuracy of 0.1% to obtain cross sections. It may be mentioned that higher excited states are generated by parametric differentiation, which goes up to sixth order in all of the present investigations. However, all of the differentiations are carried out analytically.

3. Results and discussions

State-selective electron capture cross sections and total capture cross sections for Be^{q+} (q = 1–3) + H interactions are given in tables 2–4 and the same data for B^{q+} (q = 1–4) + H interactions are provided in tables 5–8, respectively. It may mentioned that all calculated capture cross sections into each sub-shell of each partially stripped projectile ion has been multiplied by the corresponding Pauli blocking factor, determined in the same

Table 2. Total nl cross sections for Be^{+}–H(1s) ($a(b)$ denotes $a \times 10^b$).

Energy (in keV amu^{-1})	Cross sections (in 10^{-16} cm^2)							
	2s	2p	$Q(2)$	3s	3p	3d	$Q(3)$	Total
40	2.42(−1)	1.49(−1)	3.91(−1)	3.50(−2)	4.19(−2)	7.69(−3)	8.45(−2)	4.75(−1)
60	8.18(−2)	5.00(−2)	1.31(−1)	1.38(−2)	1.52(−2)	2.21(−3)	3.12(−2)	1.62(−1)
100	1.58(−2)	8.18(−3)	2.39(−2)	3.19(−3)	2.68(−3)	2.80(−4)	6.15(−3)	3.00(−2)
200	1.03(−3)	3.50(−4)	1.38(−3)	2.50(−4)	1.21(−4)	7.20(−6)	3.78(−4)	1.75(−3)

Table 3. Total nl cross sections for Be^{2+}–H(1s) ($a(b)$ denotes $a \times 10^b$).

Energy (in keV amu^{-1})	Cross sections (in 10^{-16} cm^2)							
	2s	2p	$Q(2)$	3s	3p	3d	$Q(3)$	Total
40	4.97(−1)	2.12(0)	2.61(0)	1.46(−1)	4.90(−1)	4.36(−1)	1.07(0)	3.68(0)
60	1.24(−1)	8.21(−1)	9.45(−1)	4.77(−2)	2.22(−1)	1.71(−1)	4.40(−1)	1.38(0)
100	2.60(−2)	1.79(−1)	2.05(−1)	1.01(−2)	5.60(−2)	3.04(−2)	9.65(−2)	3.01(−1)
200	4.21(−3)	1.21(−2)	1.63(−2)	1.36(−3)	4.27(−3)	1.20(−3)	6.86(−3)	2.31(−2)

Table 4. Total *nl* cross sections for Be^{3+}–H(1s) ($a(b)$ denotes $a \times 10^b$).

Energy (in keV amu^{-1})	Cross sections (in 10^{-16} cm^2)								
	1s	$Q(1)$	2s	2p	$Q(2)$	3s	3p	3d	$Q(3)$
40	2.03(−2)	2.03(−2)	1.14(0)	2.61(0)	3.75(0)	3.66(−1)	9.21(−1)	2.62(0)	3.90(0)
60	1.39(−2)	1.39(−2)	3.74(−1)	1.24(0)	1.61(0)	1.43(−1)	3.88(−1)	1.10(0)	1.63(0)
100	1.09(−2)	1.09(−2)	5.79(−2)	3.83(−1)	4.40(−1)	2.73(−2)	1.17(−1)	2.42(−1)	3.86(−1)
200	7.37(−3)	7.37(−3)	3.29(−3)	4.45(−2)	4.78(−2)	1.56(−3)	1.56(−2)	1.41(−2)	3.12(−2)
	4s	4p	4d	4f	$Q(4)$	Total			
40	1.50(−1)	4.24(−1)	8.60(−1)	6.36(−1)	2.07(0)	9.74(0)			
60	6.67(−2)	1.91(−1)	4.38(−1)	2.74(−1)	9.69(−1)	4.22(0)			
100	1.38(−2)	5.46(−2)	1.16(−1)	4.96(−2)	2.34(−1)	1.07(0)			
200	7.97(−4)	7.12(−3)	7.90(−3)	1.71(−3)	1.75(−2)	1.03(−1)			

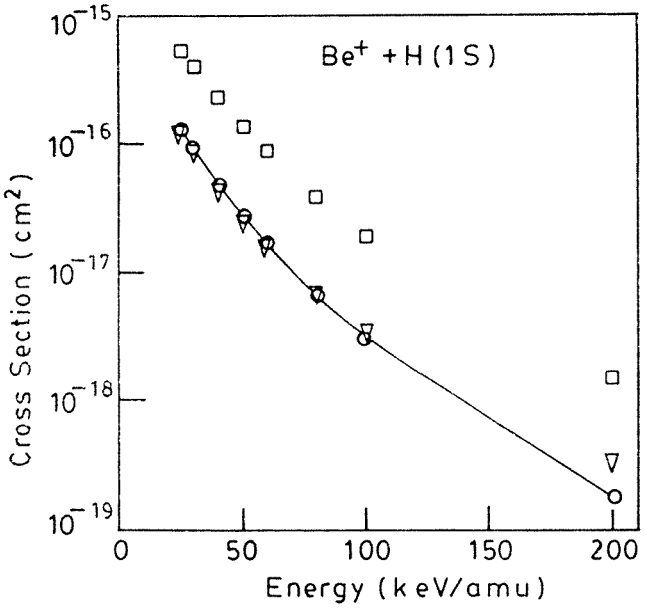

Figure 2. Total capture cross sections for $Be^+ + H(1s)$ collisions. Theory: —○—, present work with model potential; □, present work with SS model; ▽, present work with the BES model.

way as Eichler *et al* [14] and is displayed in tables. Total charge transfer cross section results for all the processes in sequences as stated are displayed in figures 2–8. Due to the non-availability of experimental data for any such process, comparisons are confined to theoretical results only. All the results given here are calculated with the post form of the interaction potential (V_f). However, we have checked for a few cases that the post–prior discrepancy lies within 15%. In order to reduce the length of the tables, numerical results in BES and SS models are not given in the tables. They are only compared in the figures.

From table 2 we find that, for the $Be^+ + H$ collision, maximum contribution comes for capture into the 2s state and the contribution from the $n = 3$ shell is dominated by 3p capture. Total cross sections are convergent within 16–20% for capture into the $n = 3$ shell over the entire energy region. From figure 2, we find that total capture cross section results

Table 5. Total *nl* cross sections for B^+–H(1s) ($a(b)$ denotes $a \times 10^b$).

Energy (in keV amu^{-1})	Cross sections (in 10^{-16} cm^2)						
	2p	$Q(2)$	3s	3p	3d	$Q(3)$	Total
25	2.00(0)	2.00(0)	1.03(−1)	1.06(−1)	2.16(−2)	2.30(−1)	2.23(0)
30	1.25(0)	1.25(0)	7.53(−2)	8.19(−2)	1.51(−2)	1.72(−1)	1.42(0)
40	5.42(−1)	5.42(−1)	4.23(−2)	4.79(−2)	7.36(−3)	9.75(−2)	6.39(−1)
50	2.57(−1)	2.57(−1)	2.53(−2)	2.83(−2)	3.86(−3)	5.74(−2)	3.14(−1)
60	1.32(−1)	1.32(−1)	1.59(−2)	1.70(−2)	2.12(−3)	3.50(−2)	1.67(−1)
80	4.15(−2)	4.15(−2)	7.09(−3)	6.70(−3)	7.13(−4)	1.45(−2)	5.60(−2)
100	1.55(−2)	1.55(−2)	3.51(−3)	2.91(−3)	2.70(−4)	6.69(−3)	2.21(−2)
200	4.93(−4)	4.93(−4)	2.63(−4)	1.26(−4)	7.06(−6)	3.96(−4)	8.89(−4)

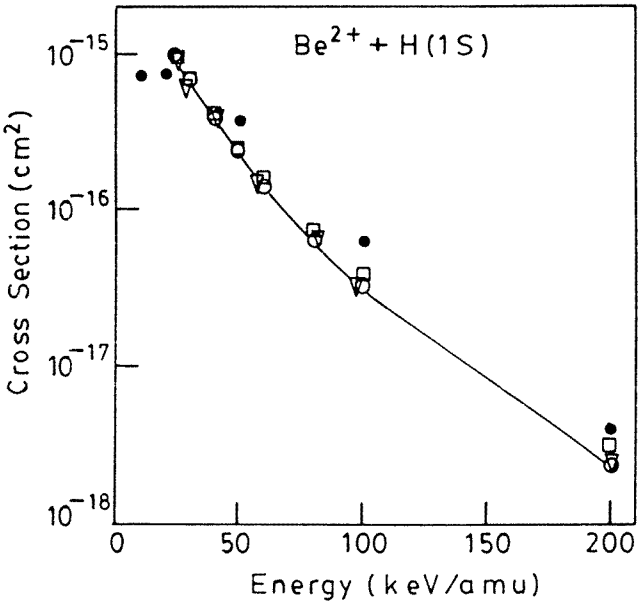

Figure 3. Total capture cross sections for Be^{2+} + H(1s) collisions. Theory: —○—, present work (model potential); □, present work (SS model); ▽, present work (BES model) and ●, CTMC results of Schultz *et al* [16].

obtained in the BES model and model potential approach are in good agreement with each other at all energies. However, results in the SS model are larger by a factor of nearly five, except at higher energies. We see from table 3 that for the Be^{2+}+H interaction, capture into $n = 3$ states contribute less than 30% to the total cross sections over the entire region. In this case, capture cross sections reach a peak value at the 2p state, which is consistent with the observations of Schultz *et al* [16]. Total cross sections (shown in figure 3), obtained using our three different approaches, are in good agreement among themselves over the entire region. However, our results are in good agreement at intermediate energy regions and disagree by a factor of two at higher energies with those of Schultz *et al* [16]. Table 4 shows the sub-shell distribution and total capture cross sections for collisions of Be^{3+} with atomic hydrogen. In this case, the maximum contribution comes from the $n = 3$ shell and capture cross sections attain a peak in the 2p state. Capture into the 3p state is dominant for

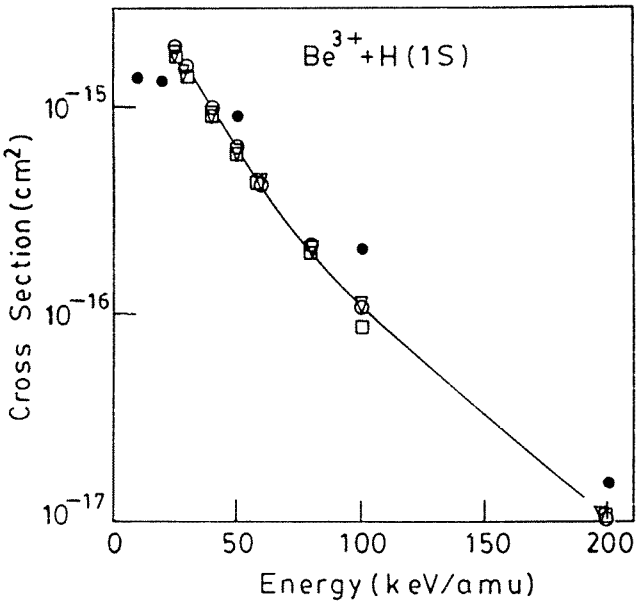

Figure 4. Total capture cross sections for $Be^{3+} + H(1s)$ collisions. Theory: —○—, present work (model potential); □, present work (SS model); ▽, present work (BES model) and ●, CTMC results of Schultz *et al* [16].

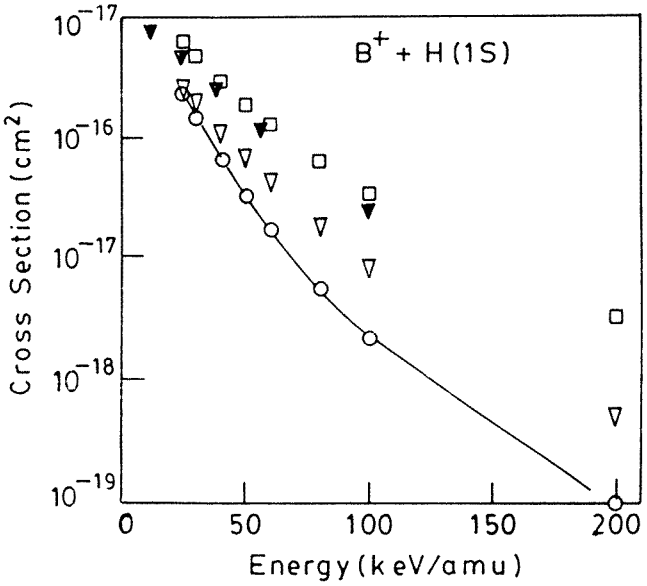

Figure 5. Total capture cross sections for $B^+ + H(1s)$ collisions. Theory: —○—, present work (model potential); □, present work (SS model); ▽, present work (BES model); ▲, the results of Hansen and Dubois [15].

contribution to $n = 3$ shell. All these observations are in agreement with those of Schultz *et al* [16]. It is evident from figure 4, that our results are in very good agreement with

Table 6. Total nl cross sections for B^{2+}–H(1s) ($a(b)$ denotes $a \times 10^b$).

Energy (in keV amu^{-1})	Cross sections (in 10^{-16} cm^2)						
	2s	2p	$Q(2)$	3s	3p	3d	$Q(3)$
25	5.74(0)	1.08(1)	1.65(1)	3.55(−1)	8.46(−1)	6.23(−1)	1.82(0)
30	3.29(0)	7.54(0)	1.08(1)	2.63(−1)	7.11(−1)	5.40(−1)	1.51(0)
40	1.18(0)	3.98(0)	5.16(0)	1.42(−1)	4.78(−1)	3.66(−1)	9.86(−1)
50	4.73(−1)	2.27(0)	2.74(0)	7.96(−2)	3.20(−1)	2.35(−1)	6.34(−1)
60	2.13(−1)	1.37(0)	1.58(0)	4.69(−2)	2.18(−1)	1.50(−1)	4.14(−1)
80	6.30(−2)	5.67(−1)	6.30(−1)	1.95(−2)	1.06(−1)	6.27(−2)	1.88(−1)
100	2.93(−2)	2.63(−1)	2.92(−1)	1.00(−2)	5.54(−2)	2.79(−2)	9.33(−2)
200	4.73(−3)	1.55(−2)	2.02(−2)	1.35(−3)	4.23(−3)	1.14(−3)	6.72(−3)
	4s	4p	4d	4f	$Q(4)$	Total	
25	1.15(−1)	2.32(−1)	2.06(−1)	4.79(−2)	6.00(0)	1.89(+1)	
30	9.54(−2)	2.15(−1)	1.92(−1)	4.23(−2)	5.44(−1)	1.28(+1)	
40	5.83(−2)	1.61(−1)	1.46(−1)	2.98(−2)	3.95(−1)	6.54(0)	
50	3.47(−2)	1.14(−1)	1.01(−1)	1.94(−2)	2.69(−1)	3.64(0)	
60	2.11(−2)	8.14(−2)	6.86(−2)	1.22(−2)	1.83(−1)	2.17(0)	
80	8.95(−3)	4.17(−2)	3.09(−2)	4.77(−3)	8.63(−2)	9.04(−1)	
100	4.54(−3)	2.23(−2)	1.44(−2)	1.94(−3)	4.31(−2)	4.28(−1)	
200	5.82(−4)	1.82(−2)	6.50(−4)	5.15(−5)	1.83(−2)	4.52(−2)	

Table 7. Total nl cross sections for B^{3+}–H(1s) ($a(b)$ denotes $a \times 10^b$).

Energy (in keV amu^{-1})	Cross sections (in 10^{-16} cm^2)						
	2s	2p	$Q(2)$	3s	3p	3d	$Q(3)$
40	1.59(0)	2.71(0)	4.30(0)	4.06(−1)	8.99(−1)	2.28(0)	3.58(0)
60	5.34(−1)	1.29(0)	1.82(0)	1.55(−1)	3.83(−1)	9.93(−1)	1.53(0)
100	8.01(−2)	3.98(−1)	4.78(−1)	2.88(−2)	1.16(−1)	2.25(−1)	3.69(−1)
200	3.60(−3)	4.58(−2)	4.94(−2)	1.59(−3)	1.55(−2)	1.35(−2)	3.05(−2)
	4s	4p	4d	4f	$Q(4)$	Total	
40	1.48(−1)	3.94(−1)	7.40(−1)	4.92(−1)	1.77(0)	9.65(0)	
60	6.62(−2)	1.82(−1)	3.92(−1)	2.28(−1)	7.68(−1)	4.21(0)	
100	1.38(−2)	5.30(−2)	1.07(−1)	4.40(−2)	2.17(−1)	1.06(0)	
200	7.96(−4)	6.98(−3)	7.57(−2)	1.60(−3)	8.50(−2)	1.64(−1)	

each other. However they are consistent with the results of Schultz *et al* at intermediate energies, but differ by a factor of two at higher energies.

From table 5, we observe that maximum cross sections come from 2p capture, and the $l = 1$ state is favoured for capture into the $n = 3$ shell. All of these characteristics are inconsistent with the results of Hansen and Dubois [15]. However, the total contribution from the $n = 3$ shell is limited to within 10%. We notice from figure 5, that our results obtained in the SS-model are in very good agreement with the total cross section results of Hansen and Dubois. This is in contrast to our other results, which disagree with each other as the projectile energy increases. Capture into the 2p state is dominant (shown in table 6) over all other sub-shells for the $B^{2+} + H$ interaction. In this case, the total contribution from the $n = 4$ shell is convergent to within 5% of the total capture cross sections. From figure 6, we find that all of our computed results are in close agreement with each other over the entire energy region. It is evident from table 7

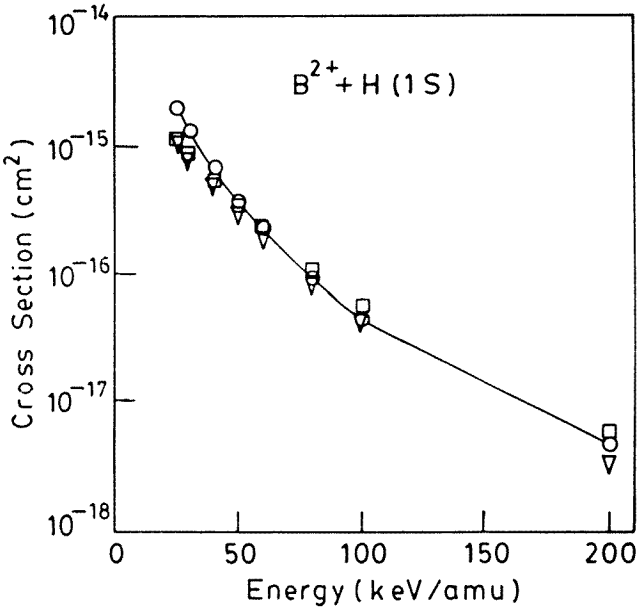

Figure 6. Same as in figure 2 for B^{2+} + H(1s) collisions.

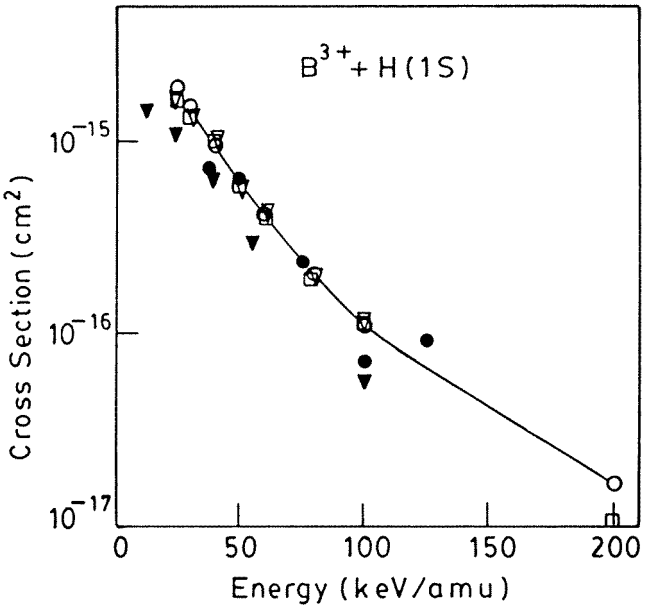

Figure 7. Total capture cross sections for B^{3+} + H(1s) collisions. Theory: —○—, present work (model potential); □, present work (SS model); ▽, present work (BES model); ▲, the results of Hansen and Dubois [15] and ●, CTMC results of Olson and Salop *et al* [13].

that the highest contribution comes from the $n = 2$ shell and therefore converges slowly, with less than 20% contribution from the $n = 4$ shell in the case of a collision of B^{3+} with the hydrogen atom. In this case capture into the $l = 2$ state is a maximum

Table 8. Total *nl* cross sections for B^{4+}–H(1s) ($a(b)$ denotes $a \times 10^b$).

Energy (in keV amu^{-1})	Cross sections (in 10^{-16} cm^2)								
	1s	$Q(1)$	2s	2p	$Q(2)$	3s	3p	3d	$Q(3)$
40	7.59(−3)	7.59(−3)	1.01(0)	1.43(0)	2.44(0)	6.19(−1)	1.97(0)	4.64(0)	7.22(0)
60	4.91(−3)	4.91(−3)	5.24(−1)	8.23(−1)	1.34(0)	2.48(−1)	6.74(−1)	2.13(0)	3.05(0)
100	2.96(−3)	2.96(−3)	1.48(−1)	3.50(−1)	4.98(−1)	6.70(−2)	1.39(−1)	5.88(−1)	7.94(−1)
200	1.99(−3)	1.99(−3)	9.70(−3)	6.73(−2)	7.70(−2)	4.83(−3)	2.09(−2)	5.15(−2)	7.72(−2)
	4s	4p	4d	4f	$Q(4)$	5s	5p		
40	2.67(−1)	7.86(−1)	1.37(0)	2.46(0)	4.88(0)	1.20(−1)	2.28(0)		
60	1.22(−1)	3.46(−1)	7.18(−1)	1.13(0)	2.31(0)	6.33(−2)	8.35(−1)		
100	3.41(−2)	8.01(−2)	2.36(−1)	2.52(−1)	6.02(−1)	1.87(−2)	2.05(−1)		
200	2.54(−3)	9.83(−3)	2.63(−2)	1.26(−2)	5.12(−2)	1.44(−3)	1.30(−2)		
	5d	5f	5g	$Q(5)$	Total				
40	6.39(−1)	9.68(−1)	5.12(−1)	4.51(0)	2.00(1)				
60	3.63(−1)	5.58(−1)	2.49(−1)	2.06(0)	9.66(0)				
100	1.22(−1)	1.52(−1)	4.73(−2)	5.45(−1)	2.64(0)				
200	1.45(−2)	9.21(−3)	1.47(−3)	3.96(−2)	2.78(−1)				

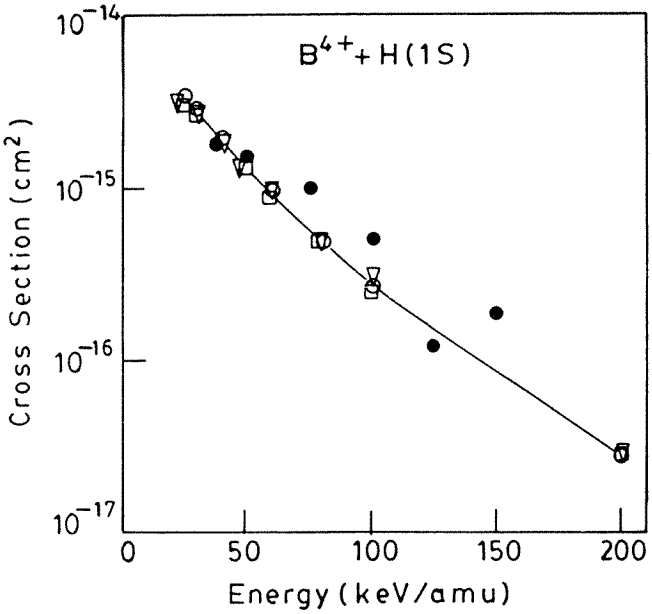

Figure 8. Total capture cross sections for B^{4+} + H(1s) collisions. Theory: —○—, present work (model potential); □, present work (SS model); ▽, present work (BES model) and ●, CTMC results of Olson and Salop *et al* [13].

for contributions from the $n = 3$ and $n = 4$ shells, respectively. This observation is in agreement with those of Hansen and Dubois. Total cross section results (shown in figure 7) are in fairly good agreement with the CTMC results of Olson and Salop [13] and those of Hansen and Dubois, except at high energies. For collisions of B^{4+} with atomic hydrogen it has been shown, in table 8, that maximum cross sections come from the $n = 3$ shell and therefore have a converging trend, with a contribution of around 20%

from the $n = 5$ shell to the total capture cross sections. The sub-shell distribution of capture cross sections has a pattern of significant contribution from the maximum angular state except for the $n = 5$ shell. Our computed results (displayed in figure 8) in all of the models have fair agreement with the CTMC results of Olson and Salop [13] for the same process.

Although we have not shown this in the tables, the cross sections are found to be maximum at the $m = 0$ state for a given value of l and n in all the cases. This corresponds to the classical picture where the electron is mostly captured into orbitals in the collisional plane. This feature is in agreement with previous findings [30]. Peak values of capture cross sections for particular values of l and n may be justified by the energy resonance of the active electron in the initial and final states. Other characteristic features may be explained in terms of Landau–Zener dynamics.

4. Concluding remarks

State-selective and total capture cross sections in collisions of different partially stripped ions of beryllium and boron with atomic hydrogen have been reported using the Coulomb–Born approximation. The CB approximation is a high-energy approximation and is valid only when the incident projectile velocity exceeds both the velocities of the bound electron before and after capture. For our investigation, the velocity of the electron in the target is well known. The velocity of the captured electron may be determined from the final state wavefunction by the Ehrenfest theorem. As the charge states of the projectiles are different, the validity of the CB approximation varies for the considered energy range. A conservative estimate may be $E_P \geqslant 40$ keV amu^{-1} except for Be^{3+} and B^{4+} ions. However, in the above-mentioned limit of energy, the sub-shell distribution of capture cross sections for Be^{3+} and B^{4+} may be reliable for $n \geqslant 2$ and $n \geqslant 3$, respectively, but the total cross sections may not be as accurate. From the computed results, we find that for ions with a charge of $q \geqslant 2$, the results are quite consistent with each other, and have fair agreement with other existing theoretical results (where available). For single charged ions, results obtained in different model potentials have pronounced disagreement. The determination of capture cross sections is sensitive to the choice of the model potential for the active electron on a projectile ion having a greater number of core electrons. For these reasons, it is very difficult to predict which model provides better results over others in the case of Be^+ and B^+ projectiles. However, results for ions with a charge of $q \geqslant 2$ may be treated as a fair estimate. Under the prevailing circumstances, more theoretical work may be carried out and experimental investigations are required for such processes.

Acknowledgments

One of us (CRM) would like to thank Department of Science and Technology (Government of India), New Delhi, India for support of this work through grant no SP/S2/L03/95.

References

[1] Bransden B H and Dewangan D P 1988 *Adv. At. Mol. Opt. Phys.* **25** 343
[2] Briggs J S and Macek J H 1990 *Adv. At. Mol. Opt. Phys.* **28** 1
[3] Fritsch W and Lin C D 1991 *Phys. Rep.* **202** 1
[4] Crothers D S F and Dubé L J 1992 *Adv. At. Mol. Opt. Phys.* **30** 287
[5] Belkic D Z, Gayet R and Salin A 1992 *At. Data Nucl. Data Tables* **51** 59

[6] Goffe T V, Shah M B and Gilbody H B 1979 *J. Phys. B: At. Mol. Phys.* **12** 3763
[7] Haugen H K, Andersen L H, Hvelplund P and Knudsen H 1982 *Phys. Rev.* A **26** 1950
[8] Janev R K (ed) 1995 *Atomic Molecular Processes in Fusion Edge Plasmas* (New York: Plenum)
[9] Bransden B H, Newby C W and Noble C J 1980 *J. Phys. B: At. Mol. Phys.* **13** 4245
[10] Crothers D S F 1981 *J. Phys. B: At. Mol. Phys.* **14** 1035
[11] Mandal C R, Datta S and Mukherjee S C 1982 *Phys. Rev.* A **28** 1144
[12] Busnengo H, Corchs S E, Martinez A E and Rivarola R D 1996 *Phys. Scr.* T **62** 88
[13] Olson R E and Salop A 1977 *Phys. Rev.* A **16** 531
[14] Eichler J K M, Tsuji A and Ishihara T 1981 *Phys. Rev.* A **23** 2833
[15] Hansen J P and Dubois A 1996 *Phys. Scr.* T **62** 55
[16] Schultz D R, Krstic P S and Reinhold C O 1996 *Phys. Scr.* T **62** 69
[17] Eichler J 1981 *Phys. Rev.* A **23** 498
[18] Dewangan D P and Eichler J 1994 *Phys. Rep.* **247** 59
[19] Dewangan D P and Eichler J 1985 *J. Phys. B: At. Mol. Phys.* **18** L65
Dewangan D P and Eichler J 1986 *J. Phys. B: At. Mol. Phys.* **19** 2039
[20] Mandal C R, Datta S and Mukherjee S C 1981 *Phys. Rev.* A **24** 3044
[21] Belkic D Z 1989 *Phys. Scr.* **40** 610
[22] Belkic D Z and Mancev I 1990 *Phys. Scr.* **42** 285
[23] Mancev I 1996 *Phys. Rev.* A **54** 423
[24] Decker F and Eichler J 1989 *Phys. Rev.* A **39** 1530
[25] Mandal C R, Mandal M and Mukherjee S C 1990 *Phys. Rev.* A **42** 1803
[26] Coulson C A 1963 *Valance* (Oxford: Oxford University Press) p 40
[27] Clementi E and Roetti C 1974 *At. Data Nucl. Data Tables* **14** 185
[28] Clark R E H and Abdallah J Jr 1996 *Phys. Scr.* T **62** 7
[29] Levis R R Jr 1956 *Phys. Rev.* **102** 537
[30] Ryufuku H and Watanabe T 1979 *Phys. Rev.* A **20** 1828